Cell Death and Differentiation (2009) 16, 1126–1134

www.nature.com/cdd

Intracellular Ca^{2+} operates a switch between repair and lysis of streptolysin O-perforated cells

EB Babiychuk*[,1], K Monastyrskaya[1], S Potez[1] and A Draeger[1]

Pore-forming (poly)peptides originating from invading pathogens cause plasma membrane damage in target cells, with consequences as diverse as proliferation or cell death. However, the factors that define the outcome remain unknown. We show that in cells maintaining an intracellular Ca^{2+} concentration $[Ca^{2+}]_i$ below a critical threshold of 10 μM, repair mechanisms seal off 'hot spots' of Ca^{2+} entry and shed them in the form of microparticles, leading to $[Ca^{2+}]_i$ reduction and cell recovery. Cells that are capable of preventing an elevation of $[Ca^{2+}]_i$ above the critical concentration, yet are unable to complete plasma membrane repair, enter a prolonged phase of $[Ca^{2+}]_i$ oscillations, accompanied by a continuous shedding of microparticles. When $[Ca^{2+}]_i$ exceeds the critical concentration, an irreversible formation of ceramide platforms within the plasma membrane and their internalisation drives the dying cells beyond the 'point of no return'. These findings show that the extent of $[Ca^{2+}]_i$ elevation determines the fate of targeted cells and establishes how different Ca^{2+}-dependent mechanisms facilitate either cell survival or death.
Cell Death and Differentiation (2009) **16,** 1126–1134; doi:10.1038/cdd.2009.30; published online 27 March 2009

Plasma membrane pores formed by cytotoxic proteins and peptides disrupt the permeability barrier in a target cell. Pathogens gain access and kill host cells by secreting pore-forming toxins, whereas the blood complement system utilises the pore-forming proteins of membrane attack complexes to eliminate both pathogens and the pathogen-invaded cells.[1,2] As in particular, cells of the blood and the vascular systems are permanently exposed to potential deadly attacks by a variety of pore-forming (poly)peptides, it is not surprising that mechanisms repairing the damaged plasma membrane have evolved.[3–6] Biological effects occurring in the wake of membrane permeabilisation and its subsequent repair are multifaceted. Apart from the two obvious end points, complete recovery or death, recovering cells can newly acquire numerous (patho)physiological functions.[3,7,8]

A rise in intracellular Ca^{2+} concentration $[Ca^{2+}]_i$ is critical for successful plasma membrane repair and cell recovery,[9,10] whereas an intracellular Ca^{2+} overload is held responsible for the death of pore-bearing cells.[11] In addition, Ca^{2+} influx, followed by transcriptional activation, is thought to induce a variety of biological responses associated with sublytic effects of pore-forming toxins.[3,4,7,8] Thus, it appears that the extent of $[Ca^{2+}]_i$ elevation following pore formation determines the fate of a targeted cell. Consequently, Morgan *et al.*[11] suggested that in nucleated cells, an initial increase in $[Ca^{2+}]_i$ stimulates the recovery processes, allowing the cell to withstand a limited complement attack. The recovery might be associated with cellular activation and the production of inflammatory modulators, which, in turn, amplify an ongoing inflammatory response.[3,11] The authors further hypothesised that a more severe membrane damage causes a sharp rise in $[Ca^{2+}]_i$, which overwhelms all recovery processes.[11] However, how $[Ca^{2+}]_i$ determines cell fate, how the acquisition of novel functions is initiated and how the 'point of no return' is defined remain unknown.

In this study, we have undertaken a simultaneous, real-time characterisation of $[Ca^{2+}]_i$ and plasma membrane dynamics in living cells permeabilised with the bacterial pore-forming toxin streptolysin O (SLO). Our data show that the fate of SLO-perforated cells is dependent on their ability to control the extent of a pore-induced elevation in $[Ca^{2+}]_i$. We detail Ca^{2+}-dependent mechanisms that elicit either repair or irreversible structural changes in the plasma membrane and show how intracellular Ca^{2+} dynamics dictate avenues that ultimately lead to cell recovery, activation or death.

Results

Our initial observations confirmed the widely accepted notion that extracellular Ca^{2+} protects cells from SLO permeabilisation:[9] a loss of cytoplasmic components owing to the presence of permanent plasma membrane pores was more pronounced in human embryonic kidney (HEK) 293 cells exposed to SLO in the absence of extracellular Ca^{2+} (Figure 1a) and was accelerated at higher SLO concentrations (Figure 1b). The analysis of individual cells revealed a high heterogeneity

[1]Department of Cell Biology, Institute of Anatomy, University of Bern, 3012 Bern, Switzerland
*Corresponding author: EB Babiychuk, Department of Cell Biology, Institute of Anatomy, University of Bern, Baltzerstrasse, 2 Bern, 3012 Switzerland.
Tel: +41 31 631 30 86; Fax: +41 31 631 38 07; E-mail; edik@ana.unibe.ch
Keywords: plasma membrane; repair; ceramide platform; microparticle; annexin
Abbreviations: SLO, bacterial pore-forming toxin streptolysin O; HEK, human embryonic kidney
Received 26.11.08; revised 06.2.09; accepted 20.2.09; Edited by B Zhivotovsky; published online 27.3.09

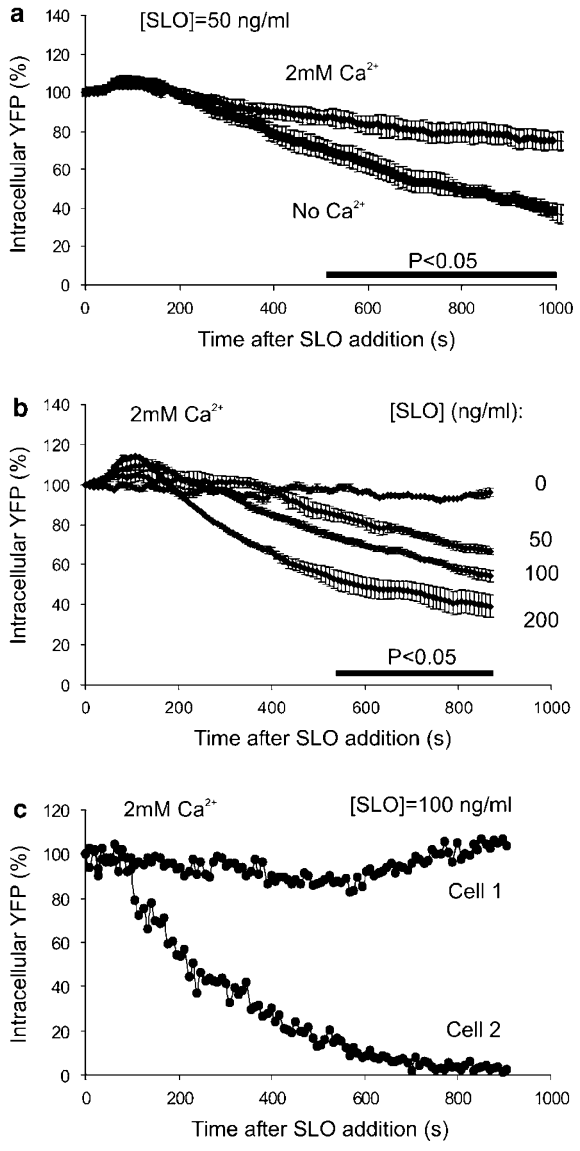

Figure 1 Loss of cytoplasmic yellow fluorescent protein (YFP) in SLO-permeabilised HEK 293 cells. (**a**) Protective effect of extracellular Ca^{2+}. SLO (50 ng/ml) was added to YFP-expressing HEK 293 cells maintained in Na-Tyrode buffer containing either 2 mM Ca^{2+} or 100 μM EGTA (no Ca^{2+}) at time point = 0. Changes in YFP fluorescence as a function of SLO exposure time were recorded by confocal microscopy from a field containing at least 10 cells. The data represent the mean ± S.E.M. (error bars) of three independent experiments. The results were analysed using the Student's *t*-test. The horizontal bar marks the times at which the differences between the two experimental conditions reached statistical significance ($P<0.05$). (**b**) The loss of intracellular YFP is accelerated at higher SLO concentrations. SLO (concentrations as indicated) was added to YFP-expressing HEK 293 cells maintained in Na-Tyrode buffer containing 2 mM Ca^{2+} at time point = 0. Changes in YFP fluorescence as a function of SLO exposure time were recorded by confocal microscopy from a field containing at least 10 cells. The data represent the mean ± S.E.M. (error bars) of three independent experiments. The results were analysed using the Student's *t*-test. The horizontal bar marks the times at which the differences between all experimental conditions reached statistical significance ($P<0.05$). (**c**) Heterogeneity of the cellular response to an SLO attack. Changes in YFP fluorescence in two individual cells recorded in the experiments described and summarised in panel b ([SLO] = 100 ng/ml) are shown to emphasise the heterogeneity of the cellular response to an SLO attack: cell 1 remains resistant to SLO permeabilisation during the course of the experiment, whereas cell 2 quickly loses its YFP contents

in their response to an SLO attack: even in the presence of extracellular Ca^{2+} some cells were heavily perforated and lost their cytoplasmic components completely, whereas others remained totally immune (Figure 1c).

In keeping with Morgan *et al.*,[11] we surmised that the outcome of an SLO attack depends on the extent of intracellular [Ca^{2+}] elevation; the activation of diverse Ca^{2+}-dependent processes at the plasma membrane enforces either cell recovery or death. Therefore, we followed the changes of plasma membrane dynamics as a function of SLO-induced elevation in $[Ca^{2+}]_i$.

$[Ca^{2+}]_i$ can be measured with cytoplasmic Ca^{2+}-sensitive fluorescent dyes in those cells that are able to repair their plasma membrane and thus retain their cytoplasmic components, but not in permanently permeabilised cells that lose their cytoplasm. Hence, we employed a novel approach that allows the assessment of $[Ca^{2+}]_i$ even in permanently permeabilised cells.[12] This method is based on the ability of the proteins of the annexin family to translocate to the plasma membrane at different $[Ca^{2+}]_i$. An efficient permeabilisation led to the elevation of $[Ca^{2+}]_i$, which we initially measured with a Ca^{2+}-sensitive fluorescent dye (Figure 2a; Fluo 3, time after SLO addition = 18 and 44 s). However, within 120 s after the addition of the toxin, Fluo 3 had completely leaked out of the permanently permeabilised cells (Figure 2a). Annexin A6, however, translocated and remained associated with the plasma membrane, provided that Ca^{2+} was present in the extracellular milieu (Figure 2a); after a washout of extracellular Ca^{2+}, annexin A6 translocated back to the cytoplasm (Figure 2a; time after Ca^{2+} washout = 60 s). Owing to its higher Ca^{2+} sensitivity,[12,13] the translocation of annexin A6 to the plasma membrane preceded that of annexin A1 (Figure 2b; compare 36 and 54 s). Immediately after its translocation, annexin A1 was evenly distributed at the plasma membrane, co-localising with annexin A6 (Figure 2c; 54 s). However, within seconds, annexin A1 segregated into lateral plasma membrane platforms, which were subsequently internalised[12] (Figure 2c; 72 s). Recently, we have established the formation and internalisation of annexin A1-positive platforms to be the result of the self-association of ceramide, generated by a Ca^{2+}-dependent activation of acid sphingomyelinase.[12] The co-localisation of annexin A1 with ceramide within the platforms was confirmed using a ceramide-specific antibody.[12] Annexin A1 and – to a much lesser degree – annexin A6 were also localised in the nucleus (Figure 2). The translocation of both annexins to the plasma membrane preceded their translocation from an intranuclear compartment to the nuclear envelope most likely due to the relative abundance of negatively charged phospholipids within the plasma membrane. The translocation of annexin A6 in SLO-permeabilised HEK 293 cells occurred at a $[Ca^{2+}]_{free} \geqslant 5\,\mu M$; however, that of annexin A1 required at least 10 μM $[Ca^{2+}]_{free}$ (Figure 2d).

Thus, using cells double transfected with fluorescently labelled annexin A6 and annexin A1, we were able to evaluate $[Ca^{2+}]_i$ in SLO-perforated cells in a three-digit mode: at a $[Ca^{2+}]_i$ below 5 μM, neither of the annexins was bound to the plasma membrane (Figure 3; cells 1 and 2; 36, 354 and 523 s, Supplementary video 1); in the 5–10 μM $[Ca^{2+}]_i$ range, annexin A6, but not annexin A1, was plasma membrane

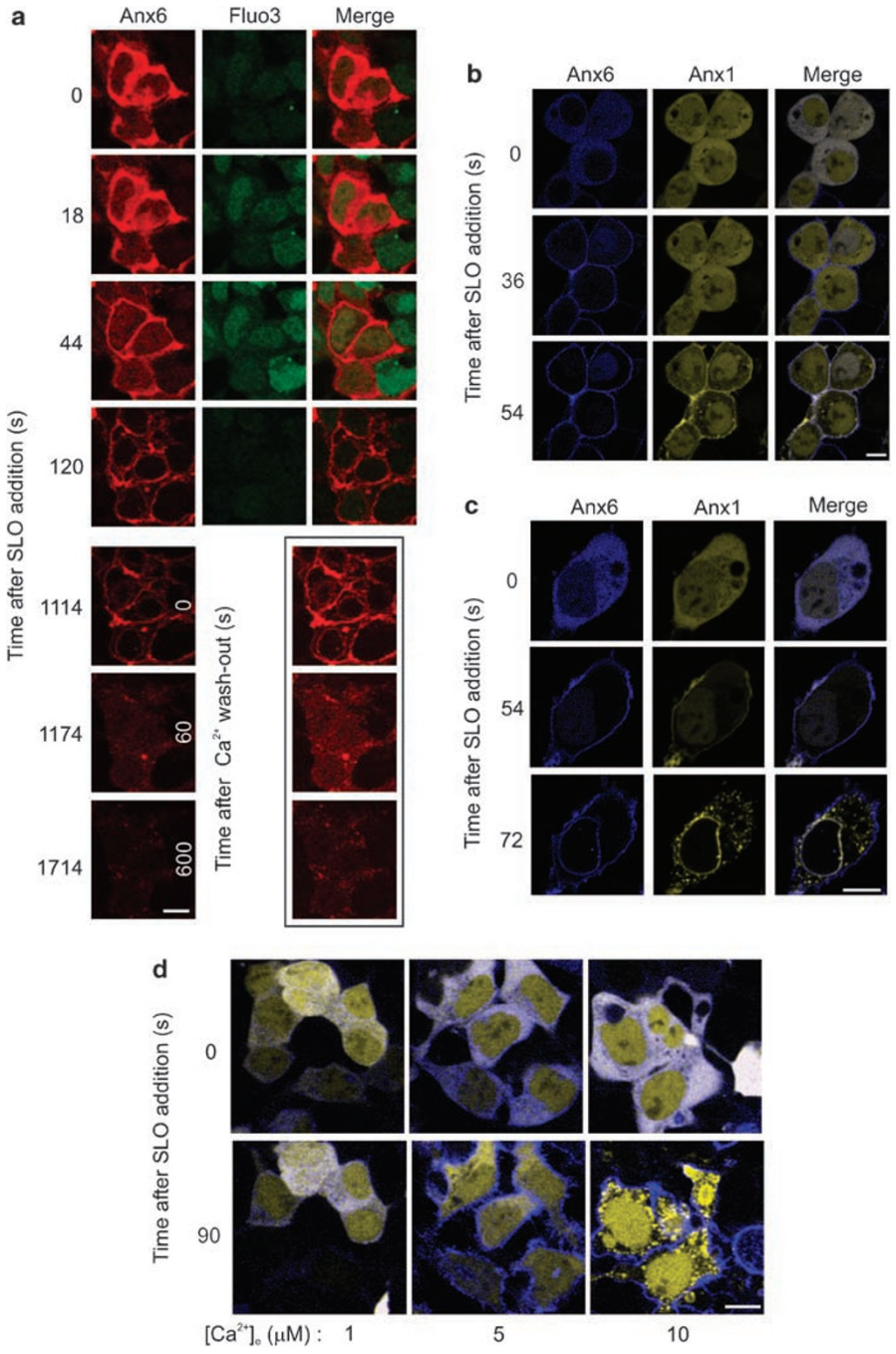

Figure 2 Ca^{2+}-dependent translocation of annexins to the plasma membrane. (**a**) Translocation and permanent association of annexin A6 (Anx6-Cherry, red) with the plasma membrane and loss of Fluo-3 (green) in SLO-permeabilised cells. SLO (200 ng/ml) was added to HEK 293 cells maintained in Na-Tyrode buffer containing 2 mM Ca^{2+} at time point = 0. At time point = 1114, the Ca^{2+}-containing buffer was substituted for the one without Ca^{2+} (time after Ca^{2+} washout = 0). In contrast to Fluo 3, annexin A6 was retained by the cells in the Ca^{2+}-containing extracellular milieu due to its binding to the plasma membrane. After a washout of extracellular Ca^{2+} (times after Ca^{2+} washout are provided on the corresponding images), annexin A6 translocated back to the cytoplasm and leaked out from the permeabilised cells. Boxed images: the intensity of the red signal in the images 'time after Ca^{2+} washout = 0, 60 and 600 s' was electronically enhanced (same enhancement for all images) to emphasise the cytoplasmic localisation of annexin A6 after a decrease in $[Ca^{2+}]$. (**b**) The translocation of annexin A6 (Anx6-CFP, blue) from the cytoplasm to the plasma membrane precedes that of annexin A1 (Anx1-YFP, yellow). SLO (100 ng/ml) was added to HEK 293 cells maintained in Na-Tyrode buffer containing 2 mM Ca^{2+} at time point = 0. Note that annexin A6 translocated to the plasma membrane after 36 s of SLO treatment, whereas the translocation of annexin A1 occurred later. (**c**) Internalisation of annexin A1. SLO (100 ng/ml) was added to HEK 293 cells maintained in Na-Tyrode buffer containing 2 mM Ca^{2+} at time point = 0. Note that after translocation, annexin A6 (Anx6-CFP, blue) and annexin A1 (Anx1-YFP, yellow) co-localised at the plasma membrane after 54 s of SLO treatment; however, only annexin A1 was internalised after its initial association with the plasma membrane. (**d**) Evaluation of $[Ca^{2+}]$ required for annexin A6 (Anx6-CFP, blue) and annexin A1 (Anx1-YFP, yellow) membrane translocation. HEK 293 cells maintained in Na-Tyrode buffer containing 1, 3, 5, 8, 10 or 50 μM $[Ca^{2+}]_{free}$ were permeabilised with SLO at time point = 0. To facilitate permeabilisation, SLO was used at a high concentration (400 ng/ml). The results obtained at 1, 5 and 10 μM $[Ca^{2+}]_{free}$ are shown. Magnification bars = 10 μm

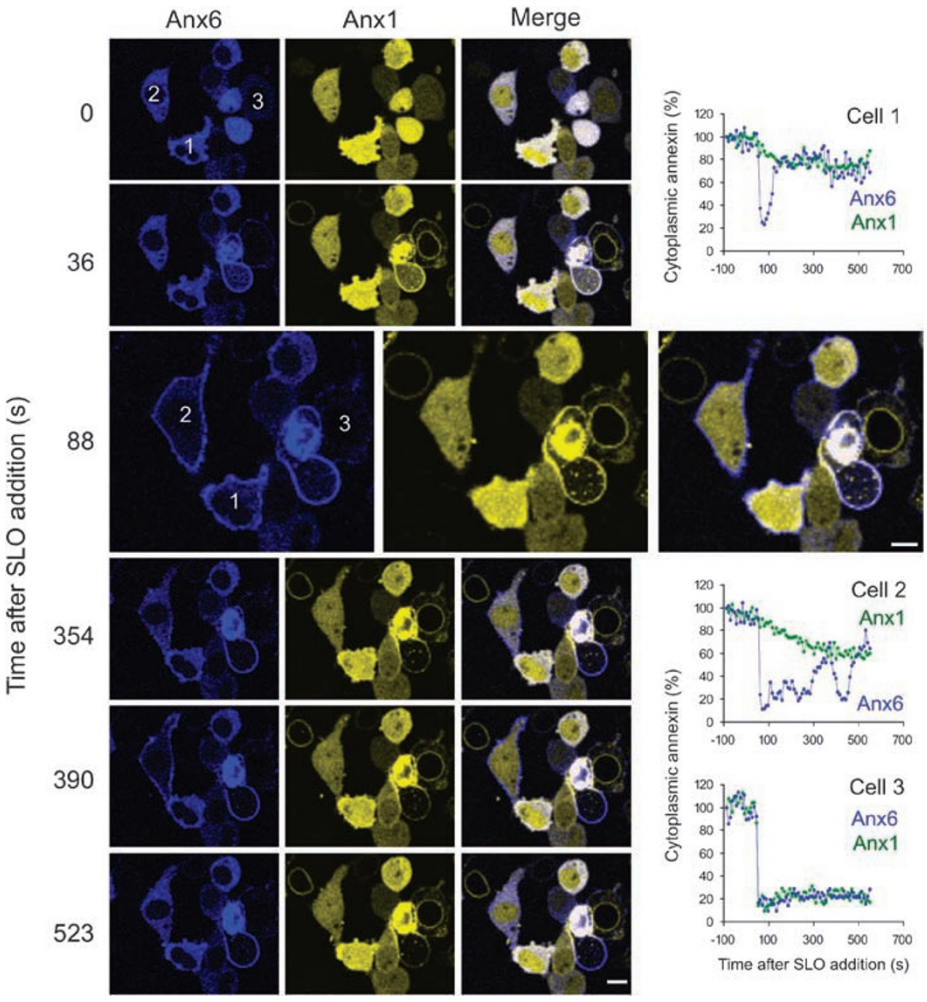

Figure 3 Evaluation of $[Ca^{2+}]_i$ by the simultaneous analysis of annexin A6 (Anx6-CFP, blue) and annexin A1 (Anx1-YFP, yellow) plasma membrane translocation following SLO permeabilisation. SLO (100 ng/ml) was added to HEK 293 cells maintained in Na-Tyrode buffer containing 2 mM Ca^{2+} at time point = 0. A set of images at time point = 88 s is presented at a higher magnification. The graphs show changes in cytoplasmic fluorescence intensity of the correspondingly numbered cells. The decrease in the cytoplasmic fluorescence corresponds to the translocation of the annexins to the plasma membrane. The translocation of annexin A6 marked cells with $[Ca^{2+}]_{free} \geqslant 5\ \mu M$, that of annexin A1 – $\geqslant 10\ \mu M$ $[Ca^{2+}]_{free}$. Magnification bars = 10 μm

associated (Figure 3; cell 2; 88 and 390 s, Supplementary video 1); and at a $[Ca^{2+}]_i$ above 10 μM, both annexins translocated to the plasma membrane (Figure 3; cell 3 at any time after SLO addition, Supplementary video 1).

The evaluation of $[Ca^{2+}]_i$ by the simultaneous analysis of annexin A6 and annexin A1 dynamics following SLO permeabilisation revealed three different outcomes for permeabilised cells. In 67 out of 186 permeabilised cells ($33 \pm 3\%$; 17 independent experiments; [SLO] = 100 ng/ml; SLO exposure = 10 min), annexin A6 dissociated from the plasma membrane after an initial translocation and returned to the cytoplasm (Figure 3; cell 1), suggesting that these cells were able to eliminate the SLO-induced pores and decrease their $[Ca^{2+}]_i$. In the vast majority of cells that had recovered (65 out of 67), annexin A1 never translocated to the plasma membrane (Figure 3; cell 1). Only in two cells that ultimately recovered, annexin A1 partially translocated; however, it resumed its cytoplasmic localisation within seconds (Supplementary Figure 1). This finding shows that, in general, recovering cells were able to confine their $[Ca^{2+}]_i$ below the point of annexin A1 translocation, that is 10 μM.

Alternatively, in $37 \pm 3\%$ of the permeabilised cells, annexin A6 remained permanently associated with the plasma membrane (Figure 3; cell 3), suggesting that these cells were unable to eliminate the SLO-induced pores and decrease their $[Ca^{2+}]_i$. In these cells, annexin A1 was inevitably membrane associated (Figure 3; cell 3), suggesting that their $[Ca^{2+}]_i$ was above 10 μM. Thus, when $[Ca^{2+}]_i$ rises above 10 μM, the cells were no longer able to repair their plasma membrane.

Finally, a number of SLO-perforated cells ($30 \pm 3\%$) entered a state in which annexin A6 repeatedly translocated between the cytoplasm and the plasma membrane, whereas annexin A1 remained always in the cytoplasm (Figure 3; cell 2, Figure 4; Supplementary videos 1,2). This finding suggests that whereas these cells could not reseal their plasma membrane completely, they were, however, capable of preventing $[Ca^{2+}]_i$ elevation over 10 μM and, as a result, entered a phase of prolonged $[Ca^{2+}]_i$ oscillations.

The balance of the outcomes for permeabilised cells was dependent on the concentration of SLO. The experiments summarised above were performed at [SLO] = 100 ng/ml. At [SLO] = 200 ng/ml (SLO exposure = 10 min;13 independent experiments), the balance was shifted in the direction of permanently permeabilised cells: only 12 ± 2% of the cells were able to recover, 76 ± 3% of the cells remained permanently permeabilised and 12 ± 2% of the cells were oscillating. At [SLO] = 50 ng/ml (SLO exposure = 10 min; five independent experiments), a large number of cells (56 ± 12%) were not efficiently permeabilised, as judged from the lack of initial annexin A6 translocation in these cells. In the rest of the cells, the balance was shifted in the direction of completely recovered cells: 64 ± 11% of the cells that showed an initial annexin A6 translocation were able to recover, 20 ± 10% remained permanently permeabilised and 16 ± 11% of the cells were oscillating. Taken together, our results imply that plasma membrane repair mechanisms operate efficiently in the 5–10 μM $[Ca^{2+}]_i$ range, but are unable to prevent irreversible cell damage if $[Ca^{2+}]_i$ rises above 10 μM.

The analysis of the annexin-decorated plasma membrane revealed that SLO-perforated, recovering cells sprout outward plasma membrane protrusions and shed them in the form of extracellular microparticles (Figures 4 and 5; Supplementary videos 2,3). The protrusions were observed in 76 ± 8% of recovering cells (14 independent experiments; [SLO] = 100 ng/ml; SLO exposure = 10 min). This number most likely underestimates the actual number of cells that were able to sprout protrusions because the detection of the protrusions was restricted to those cells residing within the confocal plane during microscopical recording. A detailed analysis of the SLO-induced plasma membrane protrusions and the microparticles revealed that they were devoid of cytoplasmic proteins but were highly enriched in annexin A1 (Figure 5). As expected for the recovering cells with a global $[Ca^{2+}]_i$ below the annexin A1 translocation point, the rest of the plasma membrane was annexin A1 negative (Figure 5). The translocation of annexin A1 to the spatially limited regions within the plasma membrane suggested that the protrusions represented 'hot spots' of Ca^{2+} entry, with local $[Ca^{2+}]$ reaching over 10 μM. They, most likely, encompass plasma membrane regions situated in the vicinity of SLO-induced pores.[14] The annexin A1-positive Ca^{2+} 'hot spots' were restricted to small regions within the plasma membrane, which suggested that the diffusion between these structures and the cytoplasm was effectively limited. Annexins are able to promote fusion of adjacent membranes in the presence of Ca^{2+}.[15] Therefore, the annexin A1–plasma membrane interaction triggered by high $[Ca^{2+}]$ within the 'hot spots' might plug (Figure 5, white arrows) or seal off (Figure 5, red arrow) the pores and prevent further $[Ca^{2+}]_i$ entry into the cytoplasm. Eventually, the annexin A1-inactivated SLO pores are shed from the plasma membrane (Figures 4 and 5; Supplementary videos 2,3).

Our results imply that the elevation of $[Ca^{2+}]_i$ above 10 μM resulted in a cell's inability to recover from an SLO attack. This failure was marked by the translocation of annexin A1 to the plasma membrane and its segregation into lateral plasma membrane platforms, which were subsequently internalised. The initial translocation of annexin A1 to the plasma membrane involves its calcium-mediated binding to the negatively charged phospholipid head groups of the membrane.[12] This mode of binding involves the C-terminal core domain of annexin A1, which contains the annexin repeats shared by all members of the annexin protein family. Lateral segregation and internalisation of annexin A1 occurs due to its binding to ceramide platforms; the unique N terminus of annexin A1 conveys this interaction.[12] Few cells, which recovered after annexin A1–plasma membrane translocation (binding of annexin A1 to negatively charged phospholipids), were able to lower their $[Ca^{2+}]_i$ before the segregation of annexin A1 (ceramide platform formation) took place (Supplementary Figure 1). Alternatively, the cells in which the formation of ceramide platforms did occur were undergoing lytic degradation marked by the loss of their cytoplasmic proteins (Figure 6). These findings suggest that neither the elevation of $[Ca^{2+}]_i$ itself nor the translocation of annexin A1 to the plasma membrane but the Ca^{2+}-dependent formation of ceramide platforms occurring at $[Ca^{2+}]_i \geqslant 10\,\mu$M represents the 'point of no return' in perforated cells.

Recently, we have shown that the inhibition of acid sphingomyelinase by desipramine decreased the Ca^{2+}-induced accumulation of ceramide and inhibited ceramide platform formation.[12] As a consequence, desipramine prevented the segregation of ceramide-sensitive annexin A1 from ceramide-insensitive annexin A6. However, it did not prevent the Ca^{2+}-induced translocation of both annexins from the cytoplasm to the cellular membranes, where they bind to negatively charged phospholipids.[12] To establish a causal link between ceramide platform formation and cell damage, we compared the extent of SLO-induced Ca^{2+} elevation in desipramine-treated and control cells. Ca^{2+} elevation, marked by the translocation of the annexins to the cellular membranes, was significantly lowered in desipramine-treated cells compared with the control cells (Figure 7). Thus, the inhibition of ceramide platform formation furnished cells with a higher resistance to SLO attack.

Annexin A1-rich plasma membrane protrusions, annexin A6 oscillations and ceramide platform formation were also observed in primary cultures of human uterus smooth muscle cells (Supplementary Figure 2). Similar to HEK 293 cells, smooth muscle cells were unable to reduce their $[Ca^{2+}]_i$ after the formation of annexin A1-positive ceramide platforms, and annexin A6 back-translocation and oscillations were observed

Figure 4 Annexin A6 oscillations and shedding of microparticles in SLO-permeabilised cells. SLO (50 ng/ml) was added to HEK 293 cells maintained in Na-Tyrode buffer containing 2 mM Ca^{2+} at time point = 0. Two sets of images are presented at a higher magnification (time points 1374 and 1463 s). The upper graph shows oscillations of annexin A6 fluorescence intensity (Anx6-CFP, blue) in the cytoplasmic region of interest (ROI 1). The decrease in the cytoplasmic fluorescence corresponds to the translocation of annexin A6 to the plasma membrane (marked by an asterisk for the upper cell). The lower graph documents the appearance of annexin A1 (Anx1-YFP, yellow) in the extracellular region of interest (ROI 2) as a result of the shedding of annexin A1-rich microparticles. RFU – relative fluorescence units. Magnification bar = 10 μm

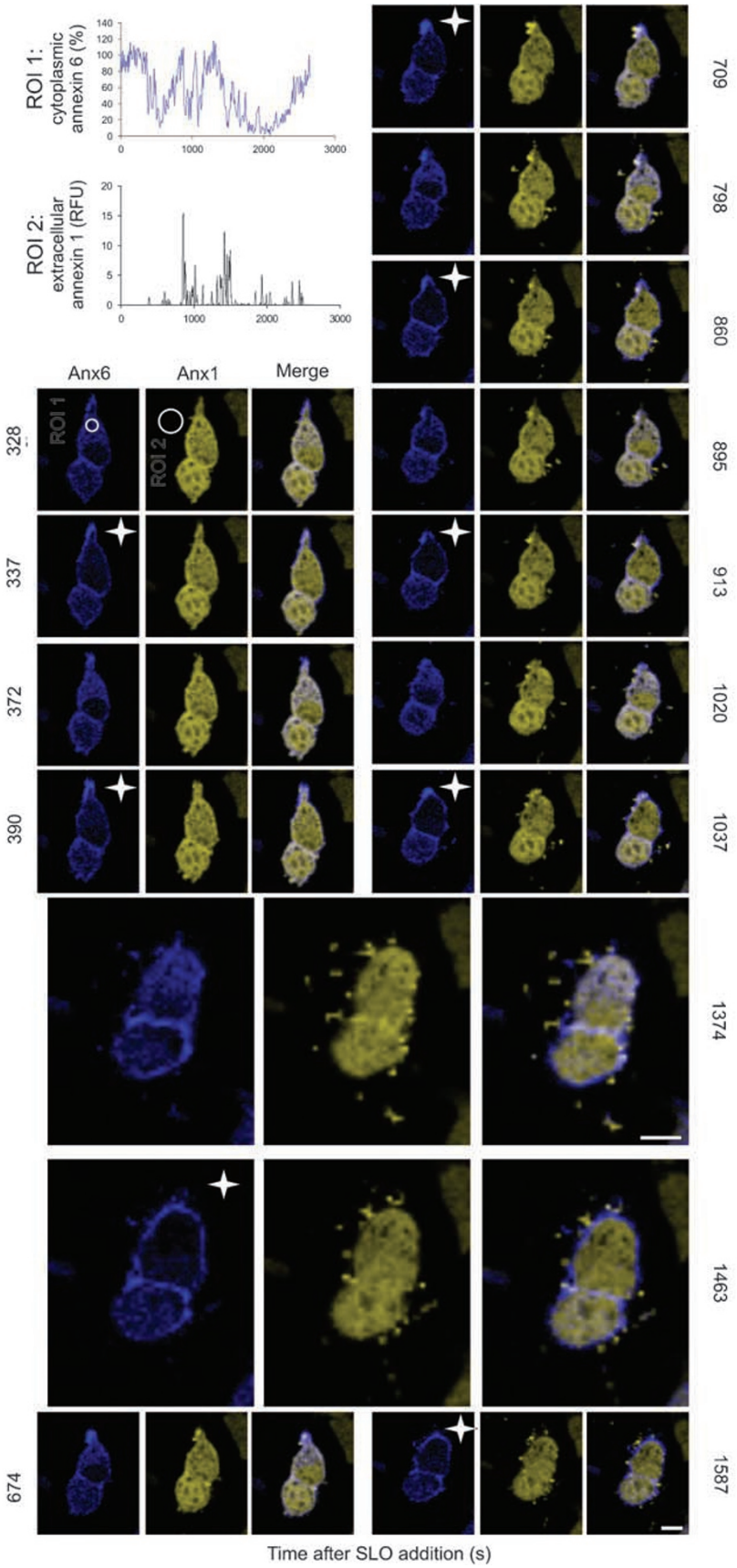
ROI 1: cytoplasmic annexin 6 (%)
ROI 2: extracellular annexin 1 (RFU)
Anx6
Anx1
Merge
ROI 1
ROI 2
328
337
372
390
674
709
798
860
895
913
1020
1037
1374
1463
1587
Time after SLO addition (s)

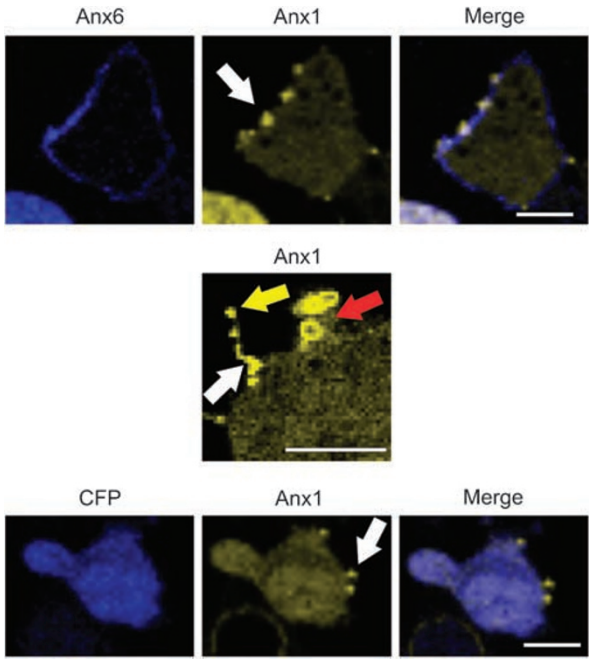

Figure 5 Annexin A1-rich protrusions (white arrows), sealed plasma membrane vesicles (red arrow) and microparticle release (yellow arrow) in SLO-permeabilised cells. Annexin A1 (Anx1-YFP, yellow), annexin A6 (Anx6-CFP, blue) and cytoplasmic cyan fluorescent protein (CFP, blue). Note that the annexin A1-rich protrusions were devoid of CFP. [SLO] = 100 ng/ml. Magnification bar = 10 μm

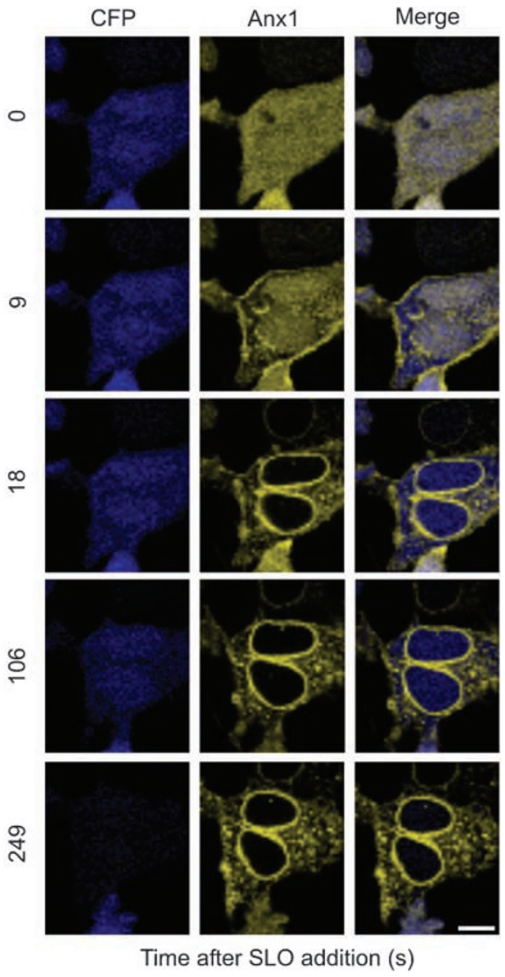

Figure 6 Loss of cytoplasmic cyan fluorescent protein (CFP, blue) after annexin A1 (Anx1-YFP, yellow) internalisation. SLO (100 ng/ml) was added to HEK 293 cells maintained in Na-Tyrode buffer containing 2 mM Ca^{2+} at time point = 0. Magnification bar = 10 μm

only in cells showing a cytoplasmic distribution of annexin A1. Primary smooth muscle cells were less sensitive to SLO attack than HEK 293 cells: only 18 ± 5% ([SLO] = 100 ng/ml; six independent experiments) of smooth muscle cells were permanently permeabilised after 10 min of SLO exposure compared with 37 ± 3% of HEK 293 cells permeabilised at the same experimental conditions ($P = 0.0003$). This can probably be attributed to the higher efficiency of Ca^{2+} extrusion by specialised contractile cells.

Discussion

Ca^{2+} signals govern a host of vital cellular functions, and are thus necessary for cell survival.[16] The prominent role played by Ca^{2+} in apoptosis is thus somewhat surprising.[17] The dual role of Ca^{2+} in the repair and killing of cells perforated by pore-forming polypeptides[18] is of particular interest as the decision on the future of the cell is made within seconds of perforation[5] and thus does not involve long-term processes, such as transcriptional activation, which otherwise might be operative during Ca^{2+}-induced apoptosis.

Our data show that the fate of SLO-perforated cells is dependent on their ability to control the extent of a pore-induced elevation in $[Ca^{2+}]_i$. We show that plasma membrane repair operating in the 5–10 μM $[Ca^{2+}]_i$ range leads to the recovery of SLO-perforated cells. Various mechanisms have been implicated in the plasma membrane repair. Endocytosis or shedding of microparticles is thought to be involved in the physical elimination of pores.[3–5] Extensively damaged regions of the plasma membrane might be patched with internal membranes delivered to the cell surface by exocytosis.[10,18] In addition, the biochemical destruction of pore-bearing membranes accompanied by simultaneous patching might be achieved by the fusion of lysosomes with the plasma membrane.[6] Our analysis confirmed that SLO-perforated, recovering cells eliminate the pores by shedding them in the form of extracellular microparticles. We detected neither endocytosis nor exocytosis of internal membranes in the recovering cells. However, annexins interact only with phosphatidylserine-rich membranes, such as the plasma membrane. Any exocytosis or endocytosis of phosphatidylserine-poor membranes will therefore escape our detection.

The importance of microparticle shedding in plasma membrane repair has been emphasised by the fact that efficient repair of SLO-induced pores occurs not only at physiological but also at low temperatures.[19] As neither endocytosis nor exocytosis is operative at low temperatures, shedding of microparticles remains the only known mechanism that is able to function under these restrictive conditions. However, a quantitative evaluation showed that, despite an efficient repair, only a fraction of SLO was removed from the plasma membrane by shedding.[19] For this reason, membrane repair at low temperatures has been partially attributed

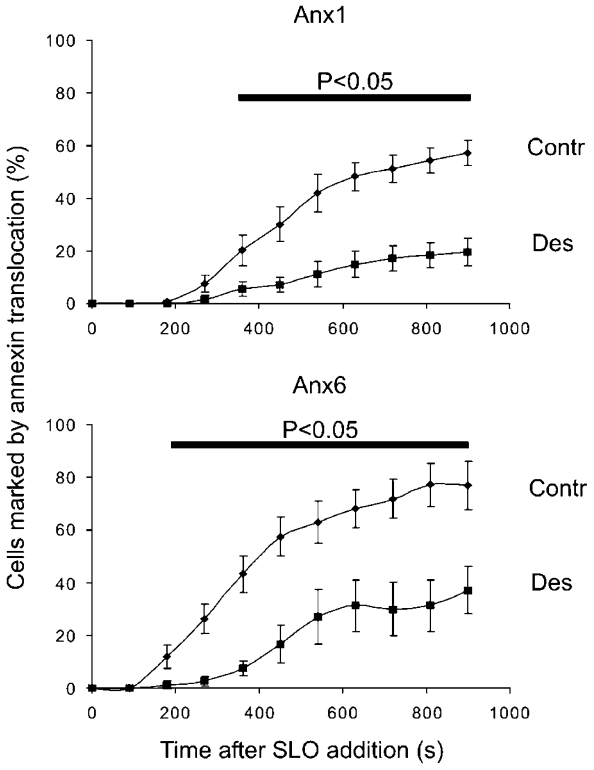

Figure 7 The inhibition of acid sphingomyelinase furnished cells with a higher resistance to SLO attack. To inhibit acid sphingomyelinase, HEK 293 cells expressing either annexin A1-YFP or annexin A6-CFP constructs were preincubated in culture medium for 2 h at 37°C in the presence of 50 μM desipramine. SLO (100 ng/ml) was added to desipramine-treated (Des) or control (Contr) cells maintained in Na-Tyrode buffer containing 2 mM Ca^{2+} at time point = 0. The SLO-induced translocation of the annexins was recorded by confocal microscopy from a field containing at least 10 cells. The number of cells in which annexin translocation had been observed was scored every 90 s and plotted (% of the cells in the observation field) as a function of SLO exposure time. The data represent the mean ± S.E.M. (error bars) of six independent experiments. The results were analysed using the Student's *t*-test. The horizontal bar marks the times at which the differences between the two experimental conditions reached statistical significance ($P < 0.05$). The higher number of cells in which annexin A6 translocation was observed is due to the higher Ca^{2+} sensitivity of annexin A6–membrane interaction compared with that of annexin A1

to microparticle shedding and partially to yet unknown mechanisms.[19] Here, we show that annexin A1 might be involved in the inactivation of SLO pores. Annexin A1 has earlier been shown to be indispensable for plasma membrane repair[20] and to play a protective role in a variety of pathological conditions.[21] Some of the annexin A1-plugged SLO pores remained within the plasma membrane of recovering cells for prolonged periods (Figures 4 and 5; Supplementary video 3). Annexin A1–plasma membrane interactions are effective both at physiological and at low temperatures.[12,22] Therefore, the annexin A1-induced inactivation of persistent SLO pores might be responsible for the discrepancy between the limited SLO removal by microparticle shedding and the efficient plasma membrane repair observed at low temperatures.[19]

Our results imply that the plasma membrane repair mechanisms are unable to prevent irreversible cell damage if $[Ca^{2+}]_i$ rises above 10 μM. We show that the Ca^{2+}-dependent formation of ceramide platforms occurring at $[Ca^{2+}]_i \geqslant 10\,\mu$M drives the perforated cells beyond the 'point of no return'. The role of ceramide platforms in the amplification of stress-induced cell death is supported by a wealth of experimental evidence,[23,24] and the accumulation of ceramide in SLO-permeabilised cells has been documented.[25]

Ceramide platforms are a prominent feature of apoptotic cells.[12,23,24] It is conceivable that ceramide platform formation is involved in the setting of the 'point of no return' not only in cells undergoing lytic degradation but also during apoptosis. By activating either survival responses or ceramide platform formation, the extent of $[Ca^{2+}]_i$ elevation in stressed cells might discriminate between healthy cells, which possess a robust metabolism and efficient Ca^{2+}-extrusion mechanisms, and the weak, underperforming cells, which were metabolically compromised even before the stress signal and thus are destined for elimination by apoptosis.

We show that the fate of SLO-permeabilised cells is not limited to two mutually exclusive options: cells, which are capable of preventing an elevation of $[Ca^{2+}]_i$ above the critical concentration, yet are unable to complete plasma membrane repair, enter a prolonged phase of $[Ca^{2+}]_i$ oscillations, accompanied by a continuous shedding of microparticles. $[Ca^{2+}]_i$ oscillations have been shown to induce a sustained cell activation, which is followed by proliferation, differentiation or the release of biologically active substances.[16,26] SLO-induced NF-κB activation and cytokine production have been documented.[7] In contrast to a physiological stimulation, the pore-induced cell activation is beyond the control of the organism and is potentially harmful. Likewise, the release of microparticles has been attributed to various pathological conditions.[27,28] Thus, the non-lethal effects of pore-forming cytotoxic agents, which are brought about by $[Ca^{2+}]_i$ oscillations, may be as important to health and disease as their extensively documented lytic properties.

Materials and Methods

Reagents. SLO from *Streptococcus pyogenes* was from Sigma. Living Colours Fluorescent protein vectors, peGFP-N1, peCFP-N1, peYFP-N1 and pmCherry-N1, were from Clontech. Restriction endonucleases, Taq polymerase and T4 DNA ligase were from New England Biolabs. Fluo-3 was from Molecular Probes. Other reagents were from Sigma.

Expression of annexins as fusions with fluorescent proteins. The coding sequences of annexin A1 and A6 were cloned into the Living Colours Fluorescent protein vectors following the PCR amplification from human bladder smooth muscle cDNA.[13]

Cell culture and transfections. HEK 293 and primary smooth muscle cells (human myometrium) were maintained in DMEM medium containing 2 mM glutamine, 100 U penicillin/ml, 100 μg streptomycin/ml and 10% FCS. Cultures of human myometrium (passages 2–4) were performed as described earlier.[29] All cells were grown in 5% CO_2 at 37°C in a humidified incubator. They were transiently transfected with plasmids using electroporation (BioRad) at 0.25 kV and analysed after incubating at 37°C for 48 h.

Imaging and intracellular calcium measurements. Unless otherwise stated, annexin A1-YFP (yellow fluorescent protein) and annexin A6-CFP (cyan fluorescent protein) were transiently expressed in HEK 293 cells. Cells seeded on glass cover slips were mounted in a perfusion chamber at 25°C in Tyrode's buffer (140 mM NaCl, 5 mM KCl, 1 mM $MgCl_2$, 10 mM glucose, 10 mM HEPES, pH = 7.4) containing 2 mM $CaCl_2$. At time point = 0, the cells were challenged with SLO. For calcium-imaging recordings, the cells were loaded for 30 min at 22°C with 3 μM

Fluo-3/AM in Tyrode's buffer. The fluorescence was recorded at 25°C with an Axiovert 200M microscope with a laser scanning module LSM 510 META (Zeiss, Germany) using a $\times 63$ oil immersion lens. Images were recorded and analysed using the 'Physiology evaluation' software package (Zeiss). $[Ca^{2+}]_{free}$ was maintained using HEDTA-Ca^{2+} buffer and calculated using MaxChelator software as described.[30]

Acknowledgements. We thank Professor Ernst Niggli (Bern) for advice and Andrea Hostettler for technical assistance. We gratefully acknowledge the financial support of the Swiss National Science Foundation (SNF grants 320000-111778 and 3100A0-121980/1 to KM and EB and the National Research Programme NRP 53 'Musculoskeletal Health-Chronic Pain' 405340-104679/1 to AD).

1. Walport MJ, Complement. Second of two parts. *N Engl J Med* 2001; **344**: 1058–1066.
2. Parker MW, Feil SC. Pore-forming protein toxins: from structure to function. *Prog Biophys Mol Biol* 2005; **88**: 91–142.
3. Morgan BP. Complement membrane attack on nucleated cells: resistance, recovery and non-lethal effects. *Biochem J* 1989; **264**: 1–14.
4. Pilzer D, Gasser O, Moskovich O, Schifferli JA, Fishelson Z. Emission of membrane vesicles: roles in complement resistance, immunity and cancer. *Springer Semin Immunopathol* 2005; **27**: 375–387.
5. Idone V, Tam C, Goss JW, Toomre D, Pypaert M, Andrews NW. Repair of injured plasma membrane by rapid Ca2+-dependent endocytosis. *J Cell Biol* 2008; **180**: 905–914.
6. Idone V, Tam C, Andrews NW. Two-way traffic on the road to plasma membrane repair. *Trends Cell Biol* 2008; **18**: 552–559.
7. Walev I, Hombach M, Bobkiewicz W, Fenske D, Bhakdi S, Husmann M. Resealing of large transmembrane pores produced by streptolysin O in nucleated cells is accompanied by NF-kappaB activation and downstream events. *FASEB J* 2002; **16**: 227–239.
8. Bohana-Kashtan O, Ziporen L, Donin N, Kraus S, Fishelson Z. Cell signals transduced by complement. *Mol Immunol* 2004; **41**: 583–597.
9. Morgan BP, Campbell AK. The recovery of human polymorphonuclear leucocytes from sublytic complement attack is mediated by changes in intracellular free calcium. *Biochem J* 1985; **231**: 205–208.
10. McNeil PL, Steinhardt RA. Plasma membrane disruption: repair, prevention, adaptation. *Annu Rev Cell Dev Biol* 2003; **19**: 697–731.
11. Morgan BP, Luzio JP, Campbell AK. Intracellular Ca2+ and cell injury: a paradoxical role of Ca2+ in complement membrane attack. *Cell Calcium* 1986; **7**: 399–411.
12. Babiychuk EB, Monastyrskaya K, Draeger A. Fluorescent annexin A1 reveals dynamics of ceramide platforms in living cells. *Traffic* 2008; **9**: 1757–1775.
13. Monastyrskaya K, Babiychuk EB, Hostettler A, Rescher U, Draeger A. Annexins as intracellular calcium sensors. *Cell Calcium* 2007; **41**: 207–219.
14. Moskovich O, Fishelson Z. Live cell imaging of outward and inward vesiculation induced by the complement c5b–9 complex. *J Biol Chem* 2007; **282**: 29977–29986.
15. Gerke V, Moss SE. Annexins and membrane dynamics. *Biochim Biophys Acta* 1997; **1357**: 129–154.
16. Berridge MJ, Bootman MD, Roderick HL. Calcium signalling: dynamics, homeostasis and remodelling. *Nat Rev Mol Cell Biol* 2003; **4**: 517–529.
17. Orrenius S, Zhivotovsky B, Nicotera P. Regulation of cell death: the calcium-apoptosis link. *Nat Rev Mol Cell Biol* 2003; **4**: 552–565.
18. McNeil PL, Kirchhausen T. An emergency response team for membrane repair. *Nat Rev Mol Cell Biol* 2005; **6**: 499–505.
19. Walev I, Bhakdi SC, Hofmann F, Djonder N, Valeva A, Aktories K *et al*. Delivery of proteins into living cells by reversible membrane permeabilization with streptolysin-O. *Proc Natl Acad Sci USA* 2001; **98**: 3185–3190.
20. McNeil AK, Rescher U, Gerke V, McNeil PL. Requirement for annexin A1 in plasma membrane repair. *J Biol Chem* 2006; **281**: 35202–35207.
21. Babbin BA, Laukoetter MG, Nava P, Koch S, Lee WY, Capaldo CT *et al*. Annexin A1 regulates intestinal mucosal injury, inflammation, and repair. *J Immunol* 2008; **181**: 5035–5044.
22. Babiychuk EB, Draeger A. Annexins in cell membrane dynamics. Ca^{2+}-regulated association of lipid microdomains. *J Cell Biol* 2000; **150**: 1113–1124.
23. Kolesnick RN, Goni FM, Alonso A. Compartmentalization of ceramide signaling: physical foundations and biological effects. *J Cell Physiol* 2000; **184**: 285–300.
24. Gulbins E, Li PL. Physiological and pathophysiological aspects of ceramide. *Am J Physiol Regul Integr Comp Physiol* 2006; **290**: R11–R26.
25. Walev I, Tappe D, Gulbins E, Bhakdi S. Streptolysin O-permeabilized granulocytes shed L-selectin concomitantly with ceramide generation via neutral sphingomyelinase. *J Leukoc Biol* 2000; **68**: 865–872.
26. Lewis RS. Calcium oscillations in T-cells: mechanisms and consequences for gene expression. *Biochem Soc Trans* 2003; **31**: 925–929.
27. Horstman LL, Jy W, Jimenez JJ, Bidot C, Ahn YS. New horizons in the analysis of circulating cell-derived microparticles. *Keio J Med* 2004; **53**: 210–230.
28. Hugel B, Martínez MC, Kunzelmann C, Freyssinet JM. Membrane microparticles: two sides of the coin. *Physiology (Bethesda)* 2005; **20**: 22–27.
29. Babiychuk EB, Babiychuk VS, Danilova VM, Tregubov VS, Sagach VF, Draeger A. Stress fibres – a Ca2+-independent store for annexins? *Biochim Biophys Acta* 2002; **1600**: 154–161.
30. Patton C, Thompson S, Epel D. Some precautions in using chelators to buffer metals in biological solutions. *Cell Calcium* 2004; **35**: 427–431.

Supplementary Information accompanies the paper on Cell Death and Differentiation website (http://www.nature.com/cdd)